Workshop on Virtual Reality Interaction and Physical Simulation VRIPHYS (2014)
J. Bender, C. Duriez, F. Jaillet, and G. Zachmann (Editors)

Mechanical Modeling of Three-dimensional Plant Tissue Indented by a Probe

Richard Malgat[1] and Arezki Boudaoud[2] and François Faure[3,1]

[1]INRIA
[2]ENS Lyon
[3]LJK-CNRS

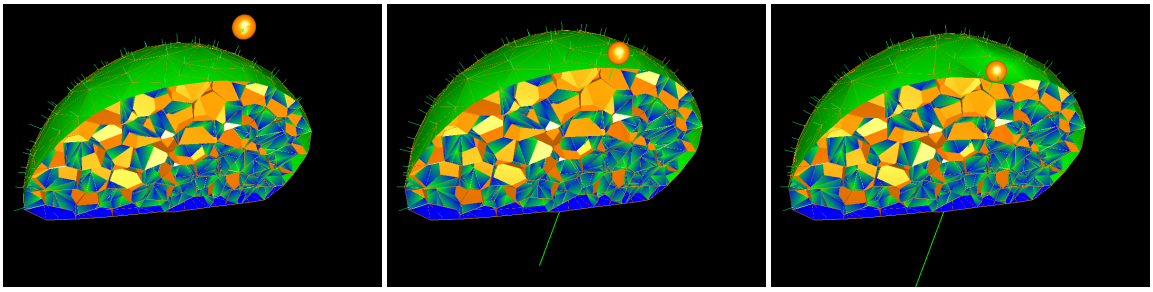

Figure 1: *Simulating nano-indentation with Atomic Force Microscopy: a spherical probe indenting a three-dimensional plant tissue.*

Abstract

Morphogenesis in a developing organism depends on the mechanics of the structural elements of the organism. In plants, typical experiments involve indenting tissues with a probe and measuring the force needed to reach a given depth. However, the heterogeneous structure and complex geometry of living tissues makes it a challenge to determine how such measurements are related to mechanical properties of the tissue, such as elastic moduli or internal pressure. Indeed, this task requires to perform a large number of direct mechanical simulations with a mesh representing the tissue. Here we propose a framework to achieve this task, using the Simulation Open Framework Architecture (SOFA) platform. We start from a realistic tissue structure corresponding to an early flower bud. We use a mesh where cells are polyhedral-shaped and are made of a liquid under pressure and where the faces separating two cells are thin elastic plates undergoing bending and stretching, and we model the interaction of this mesh with a spherical rigid probe. We obtain force versus depth curves that can be compared to experimental data. Thus our framework enables a comprehensive exploration of how mechanical parameters and probe position influence experimental outcomes, yielding a first step toward understanding the mechanical basis of morphogenesis.

Categories and Subject Descriptors (according to ACM CCS): I.3.5 [Computer Graphics]: Physically Based Modeling—

1. Introduction

Understanding morphogenesis, i.e. how organisms achieve their final shape, is a scientific challenge that requires the input of many disciplines. Gene activity prescribes shape [CRLM*04], but only indirectly since shape is determined by the mechanical elements of the organism [MDBH11]. Plants are well-suited to investigate morphogenesis because their mechanics is dominated by a single type of mechanical element, the cell wall [Nik92].

DOI: 10.2312/vriphys.20141224

Accordingly it is essential to quantify the mechanics of cell walls, which, following experiments, depends on the parametrization of mechanical models of tissues interacting with probes [MBB13, RKS13]. However, available models address only simple geometries such as a single cell [VAVB12b] or a single cell layer [KWK*12]. Indeed full 3D models involve thousands of degrees of freedom, and the exploration of the parameter space requires a number of direct simulations that grows exponentially with the number of parameters, raising the issue of the trade-off between precision and speed of simulations. We believe that Computer Graphics simulation libraries are well adapted for this, and we present an efficient computational framework to model the mechanics of three-dimensional plant tissues indented by a probe.

A plant tissue can be viewed as a tiling of a region of space by cells that are approximately polyhedral and have a size of a few micrometers. Each cell can be modeled as a liquid under pressure, which is in the range 0.1–1MPa [Nik92]. This pressure is contained by cell walls, which can be modeled as thin elastic plates (thickness 0.1–1μm) made of a polymeric material (elastic modulus in the range 1MPa–1GPa), and which lie at the faces of the polyhedra. Early mechanical measurements relied on macroscopic experiments that yield the (apparent) elastic modulus of a tissue at a macroscopic scale [Nik92].

In order to obtain mechanical properties at a cellular resolution, experiments have been scaled down [Gei06, RKS13, MBB13], notably by using micro- or nano-indentation methods, wherein a micrometric or nanometric probe indents the surface of the tissue while force and displacement are measured. These indentation methods are named according to how displacements are controlled and forces are measured; Cellular Force Microscopy [KWK*12] was designed for slightly larger displacement/forces than Atomic Force Microscopy (AFM), which is more suited to small scale / small force measurements [PBG*11, RSD*09, MGT*11, FCS*12, RRS*12, MMC*14]. If the tissue were a continuous, homogeneous elastic body, it would have been straightforward to deduce elastic modulus from indentation experiments using standard contact mechanics [Joh87]. However, as plant tissue is heterogeneous and is full of liquid-filled cavities, experimentalists need to resort to (sometimes unverified) assumptions, for instance that the size of the probe enables the measurement of local (e.g. wall-level) or global (e.g. cell-level) properties of the tissue.

Analytical mechanical models were developed to go further, but they are limited to simple configurations, such as the indentation of inflated thin shells that are spherical [VAVB12b] or ellipsoidal [VAVB12a], or the indentation of a continuous elastic half-space with elastic modulus depending on the distance from its plane surface [LBT08]. Moreover, it appears that the determination of the field of elastic moduli in a body from indentation experiments is ill-posed, unless additional assumptions are made, such as homogeneity [Joh87], simple gradation of properties [LBT08] or existence of two types of materials [RSD*09]. Therefore there is a strong need for realistic and efficient computational mechanical models than enable a comprehensive exploration of the parameter space. The more advanced studies addressed a single layer of plant cells with a sub-wall resolution [KWK*12], but such sub-wall resolution prevents a comprehensive investigation of the parameter space.

Unlike previous studies, we address here the indentation of realistic three-dimensional tissues. To do so, we use the Simulation Open Framework Architecture (SOFA) software, an open source library designed for physically based simulations in the field of medical simulation and computer graphics [FDD*12]. We illustrate our approach on the structure of the early floral meristem, which is a very young flower bud in the shape of a dome attached to the side of the shoot, and which consists of a few hundred cells in the plant Arabidopsis. The model accounts for the cellular structure of the floral meristem [FDM*10, BCA*14], for cellular pressure, for the mechanics of the cell walls considered as thin elastic plates undergoing stretching and bending, and for the indentation by a spherical probe. We use the same tissue structure as in [BCA*14], but instead of modeling tissue growth, we refine the mechanical model (e.g. by adding bending) and we consider the indentation of the tissue. In the following, we present the details of the structure and the model, a validation of the model, and then results that are discussed in the light of available experiments.

2. Realistic structure of meristem

We reused a tissue structure obtained in [BCA*14]. Briefly, this structure was derived as follows. A floral meristem (a young flower bud) from the plant Arabidopsis was imaged from confocal microscope and reconstructed in 3D in [FDM*10]. Then the 3D image was segmented in small volumes corresponding to cells [FDM*10]. Due to the noisy nature of the original images, such segmentation cannot be directly transformed directly in a mesh usable in a mechanical model. Therefore, a Voronoi tessellation of 3D space was constructed from the centers of mass of all cells: the faces of polyhedra are defined from all points that are equidistant to two centers of mass, as schematized in 2D in Figure 2. In addition this mesh was closed using the surface of the segmented floral meristem. Thus, [BCA*14] obtained a 3D tessellation where each polyhedron corresponds to a cell from the original floral meristem.

We triangulated all faces to obtain our simulation mesh. In view of the trade-off between precision and speed of simulations, we chose to use a mesh with the minimal number of triangles, except near the point of impact of the indentor where the triangles were subdivided 16 times in order to improve precision where the model is most deformed. Overall, the mesh consists of 500 polyhedra (cells) with 3000 ver-

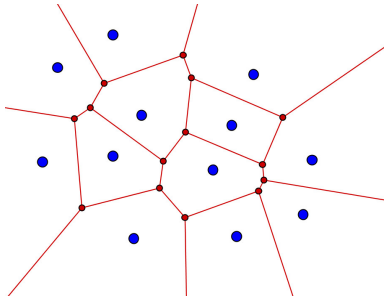

Figure 2: *2D Voronoi tesselation*

tices, and more than 11000 triangles, each cell wall measuring between 5 to 10 units of length for a whole structure of around 80 units (see table 10). The radius of the spherical tip of the probe measures between $\frac{1}{15}$ of a cell size to half a cell size. Figure 3, shows the floral meristem imaged by confocal microscopy (left, [FDM*10]), the inside of the simulated structure (right), and its whole structure together with the simulated spherical AFM (bottom). The blue part is considered to be fixed since it is linked to the stem.

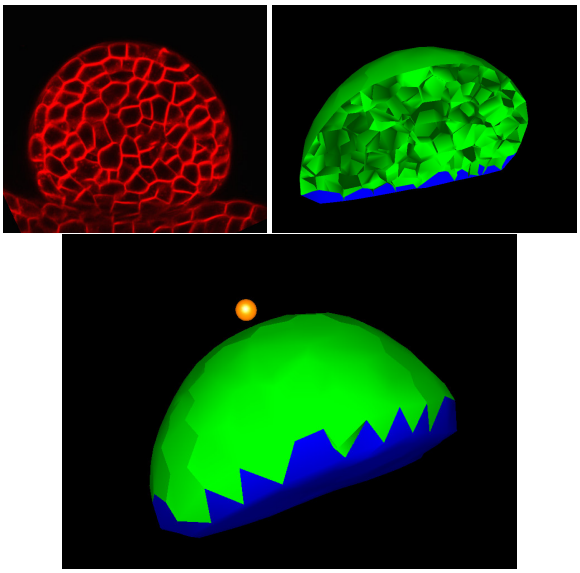

Figure 3: *Realistic structure of a meristem: top view of a flower bud with cell contours marked in red; mechanical structure generated; simulation of a spherical probe indenting the structure*

3. Mechanical Modeling

The SOFA framework allows us to divide the simulation into several components, represented in a graph as in Figure 4. At the root of this graph are the default components controlling the animation and the detection collision. A time integration solver which compute the dynamics of the whole simulation, associated with a linear solver is added to this node, as well as all our degrees of freedom which correspond to the vertices of the mesh.

Then the meristem topology is filled with our triangulated structure and the mass and bending force field, which are acting on the whole meristem are to be found here. Then the node split in two parts : the surface with the pressure and the stretching, and the interior which reacts on stretching, but not pressure.

Finally, a simulated AFM (a rigid sphere) enters in contact with the structure.

The main elements of this graph: the time integration method, the finite elements representing the stretching, the pressure, and the bending force field are described thereafter.

Each child node whose mechanical structure (i.e. vertices, deformation gradient...) relies on the displacement of its mechanical parent, is displaced via what we call mapping and is described in Section 3.2.1.

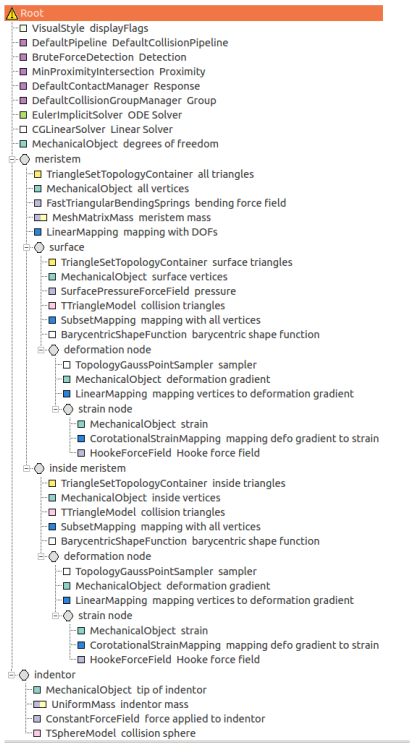

Figure 4: *Our Sofa Graph*

3.1. Time Integration

Our physical vertex-based model undergoes forces and the corresponding displacements are computed by solving partial differential equations. Based on the work of [BW98], we use a full implicit Euler solver (coupled with a conjugate gradient solver), which gives us the equations of motion through the corresponding forces. Each vertex has some coordinates x_i and velocity $\dot{x}_i = v_i$. If we denote by $x = (x_i)_{i=1...n}$, the principle of the dynamics yields the following general equation:

$$\frac{d}{dt}\begin{pmatrix} x \\ \dot{x} \end{pmatrix} = \frac{d}{dt}\begin{pmatrix} x \\ v \end{pmatrix} = \begin{pmatrix} v \\ M^{-1} f(x,v) \end{pmatrix} \tag{1}$$

with M the mass matrix and f a function dependant on the displacements and velocities. The implicit backward Euler method then writes, with a spatial discretisation:

$$\frac{d}{dt}\begin{pmatrix} \Delta x \\ \Delta v \end{pmatrix} = \tau \begin{pmatrix} v_0 + \Delta v \\ M^{-1} f(x_0 + \Delta x, v_0 + \Delta v) \end{pmatrix} \tag{2}$$

A first order Taylor expansion in f is given by:

$$f(x_0 + \Delta x, v_0 + \Delta v) = f_0 + \frac{\partial f}{\partial x}\Delta x + \frac{\partial f}{\partial v}\Delta v \tag{3}$$

and solving for v, this can be rewritten as:

$$(\mathbf{I} - \tau\,\mathbf{M}^{-1}\mathbf{D} - \tau^2\mathbf{M}^{-1}\mathbf{K})\Delta v = \tau\mathbf{M}^{-1}(f_0 + \tau\mathbf{K}v_0) \tag{4}$$

where τ denotes the time step, $\mathbf{K}$ the stiffness matrix ($\mathbf{K} = \frac{\partial f}{\partial x}$) and $\mathbf{D}$, the damping matrix ($\mathbf{D} = \frac{\partial f}{\partial v}$). To enter in more detail the derivation, we refer the reader to [BW98].

We have chosen $\mathbf{D}$ as the popular Rayleigh assumption: $\mathbf{D} = \alpha\mathbf{M} + \beta\mathbf{K}$. But notice that, as we are seeking a static solution, the displacement of the tip of the AFM induced by a certain amount of force, the influence of $\mathbf{D}$ is negligible.

The mass matrix is lumped and dependent on the mesh: for each triangle, we compute the mass by multiplying the mass density by the area of the triangle and report one third to each vertex.

The stiffness matrix depends on each force field, i.e. finite element, pressure, bending, and is computed for each force field. In the general form, it can be written as:

$$\mathbf{K}_{ij} = \frac{\partial f_i}{\partial x_j}$$

with

$$f_i = -\frac{\partial W}{\partial x_i}$$

with W being the potential energy of the corresponding force field.

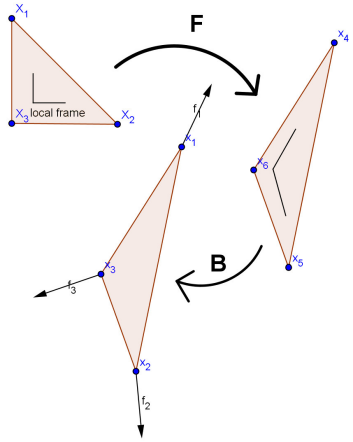

Figure 5: *classical implementation of finite element*

3.2. Finite Element force fields

Each cell wall of the meristem is triangulated and has an associated finite elements force field, representing the stretching of the structure, i.e. the forces and displacements in the plane of the element. The usual way to compute some triangular finite element, as stated in [ZC67], is to compute the forces acting on each vertex of the triangle from the displacements of these vertex, through the deformation gradient of the element as shown in Figure 5. Usually we start with the displacements of the 3 vertices, then we compute the deformation gradient of the element, $\mathbf{F} = \frac{\partial x}{\partial X}$ with x the displacement of the vertices and ∂X refers to the spatial differentiation. Then the strain measure, which is, in our model a corotational strain

$$\varepsilon = \frac{1}{2}[\mathbf{R}^T\mathbf{F} + \mathbf{F}^T\mathbf{R}] - \mathbf{I} \tag{5}$$

with $\mathbf{R}$ being the rotational part of the deformation gradient $\mathbf{F}$.

Then from this strain, we calculate the stress thanks to a material law like the isotropic Hooke's law that we have used combined with a corotational strain.

$$\sigma = \lambda tr(\varepsilon)\mathbf{I} + 2\mu\varepsilon \tag{6}$$

with λ and μ the Lame coefficients.

Finally, applying the transposed of the strain-displacement matrix usually called B to the stress converts this stress into forces : $f = B^T\sigma$.

This computation is decomposed in several layers in the SOFA framework. Instead of applying the transposed of the strain-displacement matrix to the stress, which gives us directly the forces per vertex, the stress tensor produces a generalized force at the deformation gradient level, which is

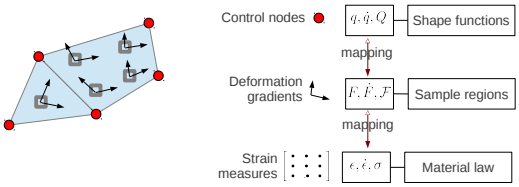

Figure 6: *three levels of hierarchies in FE force field*

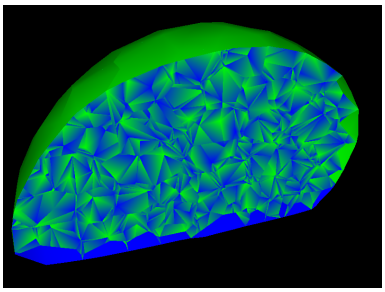

Figure 7: *finite element modeling*

in turn converted to vertex forces. The communications between layers are called *mappings* (a generalization of hard bindings introduced by [SSIF07]). The computations traverse the layers up and down as shown in Figure 6. This allows more flexibility in the implementation, since we can change only one component in the SOFA graph, to choose, for instance, a non linear material law instead of a isotropic Hooke's law at the bottom layer, or a Green Lagrange strain instead of a corotational strain as mapping between the middle and bottom layer.

The total stretching energy is given by :

$$W = \frac{1}{2}\int \varepsilon \cdot \sigma \tag{7}$$

Therefore the integrated stress is given by $\frac{\partial W}{\partial \varepsilon}$ and the associated forces on the vertices of our elements are given by:

$$f = -\frac{\partial W}{\partial x} = -\frac{dF}{dx}^T \frac{d\varepsilon}{dF}^T \frac{\partial W}{\partial \varepsilon} \tag{8}$$

Then then generalized forces undergone by the stress tensor take the form $\frac{\partial W}{\partial \varepsilon}$, which is the integrated stress, and these forces are moved upward to the parent degrees of freedom (i.e. the vertices located at the top of this hierarchy) by the transpose of the Jacobian: $\frac{d\varepsilon}{dF}^T$, and $\frac{dF}{dx}^T$.

Without any prior knowledge on cell wall properties, we have chosen to implement a uniform isotropic elastic material.

3.2.1. Mappings

We use the mappings between each levels of the SOFA scene graph. These elements allow to compute the coordinates of a child with respect to one or more parent coordinates. The independent degrees of freedom (DOF) are on the top of the hierarchy. The mapping relation writes :

$$x_c = \mathcal{J}(x_p(t), X) \tag{9}$$

with X the initial mechanical state.

The velocity at the child level is given by the jacobian of the mapping :

$$v_c = J v_p \tag{10}$$

with $J = \frac{\partial \mathcal{J}}{\partial x}$. Note that the positions and velocities are propagated top-down (from parents to children), while forces are moving bottom-up. The principle of virtual work states that the power of the force must be the same at the two levels, which gives the following relation :

$$f_p = J^T f_c \tag{11}$$

Mass and stiffness matrices can be transferred bottom-up. For instance, if the mass matrix is defined at the child level $\mathbf{M}_c$, its counterpart at the parent level is defined by : $\mathbf{M}_p = J^T \mathbf{M}_c J$.

3.3. Pressure force field

In addition to the finite elements model, we add inner turgor (hydrostatic) pressure, making the assumption that the pressure is regulated by the plant so that it is uniform in all the cells. This is equivalent to applying the pressure only on the surface elements. We thus apply a force to each vertex that is proportional to the area of the triangle considered and also proportional to turgor pressure, directed along the normal to the element (See Figure 8).

The force applied to vertex i is thus given by :

$$P_i = \frac{1}{3} A_j p \tag{12}$$

with A_j the area of the triangle j to which the vertex i belongs, and p the constant turgor pressure in the floral meristem.

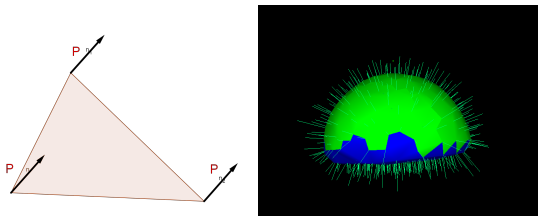

Figure 8: *Meristem with pressure represented by arrows*

3.4. Bending force field

Finally, computing the bending energy reveals that at low pressure (in plasmolyzed state), bending cannot be negligible. Therefore we implemented the bending model of [PMT06], which remains quite accurate for low bending, with low computational cost. In [PMT06] the bending is represented via linear springs depending on the curvature between two elements. Their idea is to compute a "bending vector" linearly dependent of the vertices positions. This vector is then applied as a force proportionally to the bending stiffness of the surface.

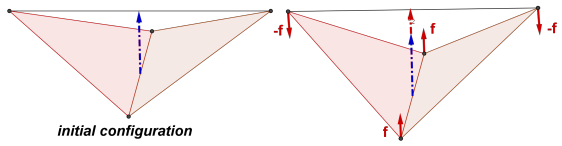

Figure 9: *linear bending*

This model introduces a bending stiffness, which acts linearly on the forces per vertices. As we are seeking physical parameters, this stiffness must not be chosen arbitrarily, but rather defined from properties of the cell walls.

To scale this bending stiffness, we restart from the equations of elastic thin shells [LL70], from which we get the moment per unit of length of bending forces applied to a shell:

$$M = \frac{Eh^3}{12(1-\nu^2)}\gamma \tag{13}$$

with E the young modulus, h the thickness of the shell, ν the poisson ratio and γ the radius of curvature. This can be put in correspondance with [PMT06] where the moment is given by:

$$M' = l\mu\gamma \tag{14}$$

with l the length of the edge between two adjacent triangles, μ the bending stiffness.

By identification the bending stiffness is:

$$\mu = \frac{Eh^3}{12(1-\nu^2)} \tag{15}$$

3.5. Simulated AFM

Our simulated AFM is a simple sphere of diameter comparable to cell size. We apply a given force in one direction orthogonal to the meristem and we quantify the depth reached by the sphere at equilibrium.

3.6. Physical parameters

The main physical parameters of the simulation are summarized in table 10. Two different sets of independent parameters constitute our model : on the one hand, the geometrical parameters (cell length, cell wall thickness), and on the other hand, the material parameters (Young modulus, Poisson ratio, pressure constant and bending stiffness).

We have scaled our parameters, in order to respect the ratio of experimental data.

$$1 \leq \frac{E}{P} \leq 1000, \quad \frac{L}{h} \approx 0.1$$

with L the size of a cell, and h the thickness of its wall. The poisson ratio was chosen so that the material is almost incompressible, while the bending stiffness was calculated according to equation 15.

4. Validation in a simple case

To validate our method, we implemented Atomic Force Microscopy on a single plane shell, for which we can compare our curves to analytical results. This simplified model also allows us to find the good trade-off between precision and rapidity of the simulation, as it enables us to tune different criteria, as the number of subdivision steps for the triangles indented, or the precision at which we stop the simulation. The typical dimensions of the plane are that of a cell in the meristem mesh.

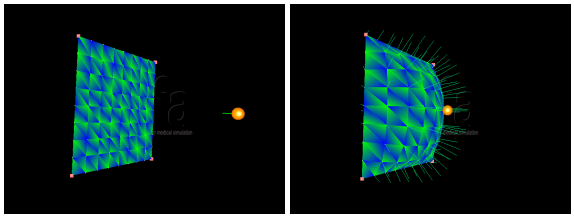

Figure 11: *Simplified model used for validation, without and with pressure*

Our simplified model is a square plate undergoing stretching and possibly submitted to a pressure force pressure (Figure 11) and the AFM indentor is also represented as a sphere. This simplified model does not take any bending into account since we want to compare it to analytical formulae from the literature.

In Figure 12 the sensitivity to the pressure can be seen. The force-displacement curves are straight lines when the plate is submitted topressure, which is in agreement with the analytical model in [VAVB12a], and the slope of these lines depends on the value of pressure; whereas Figure 13 shows that, with zero pressure the curve is well approximated by cubic function cx^3, which is in agreement with the analytical model given in [LL70].

	Young modulus (E)	Pressure (P)	Poisson ratio (ν)	Bending stiffness (μ)	cell length (L)	wall thickness (h)
model	50 - 1000 Pa	0 - 40 Pa	0.49	1.8 - 35 J	5 - 10 m	0.7 m
experimental	1 - 1000 MPa	0.1 - 1 MPa	unknown	unknown	5 μm	0.1 - 1 μm

Figure 10: *Table of typical physical parameters*

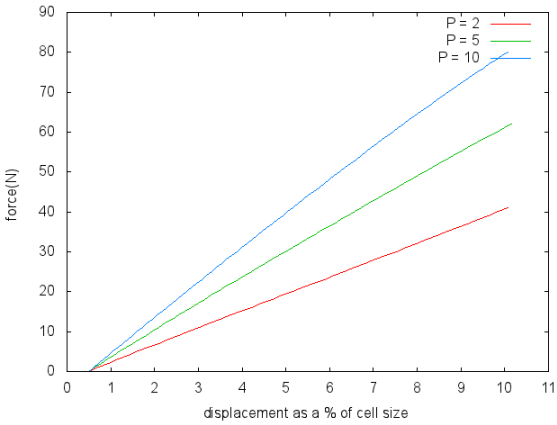

Figure 12: *Sensitivity of curves to pressure*

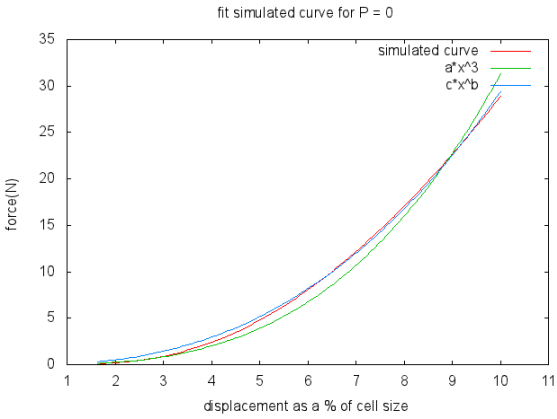

Figure 13: *Curves without pressure fitted by polynomials*

Thus, the simplified model captures the properties of the structure, i.e. the internal pressure and the elastic modulus of the cell walls. The indentation process is also completely reversible as we have chosen to implement an elastic law (Hooke's law for the finite elements) as can be seen in Figure 14: the curve representing indentation almost perfectly matches the de-indentation one, which also demonstrates the convergence of the simulations.

An other advantage of this structure is that it allows us to tune parameters such as the criteria to stop simulations (see Figure 15): when the positions and velocities of the vertices

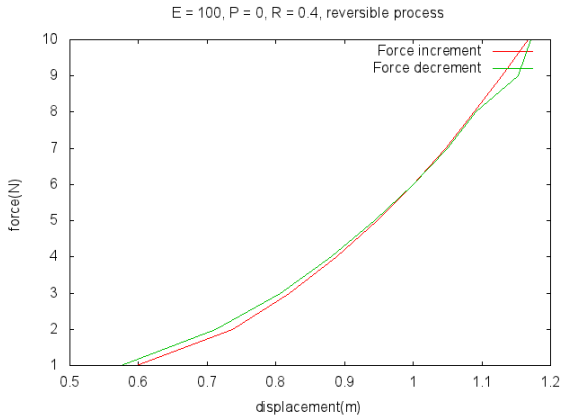

Figure 14: *process is reversible as indentation matches de-indentation*

of our model drop below threshold values, we stop the simulation. As can be seen in Figure 15, the precision needed is at least 10^{-3}m while a typical cell size is between 5 and 10m, and the whole meristem structure is around 80m.

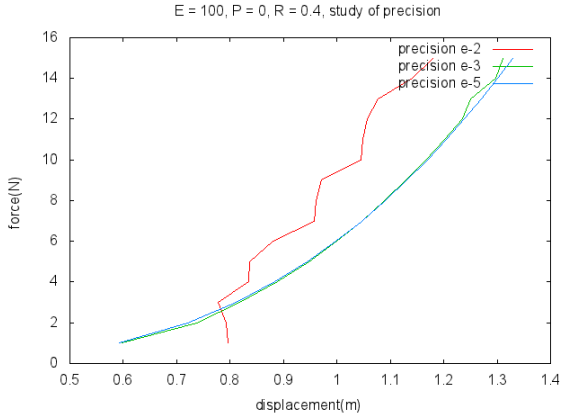

Figure 15: *sensitivity of curves to precision criteria*

For the subdivision of the triangles of the mesh, we have tried different levels of refinement, (as can be seen in Figure 17) and followed the process described in Figure 16. Each original triangle is split into 4 smaller triangles, whose vertices are the original vertices and the middles of the original triangle's edges. The geometrical properties of the

subidived topology is closed to the previous one and does not lead to degenerate triangles (having great disparity in edges' length).

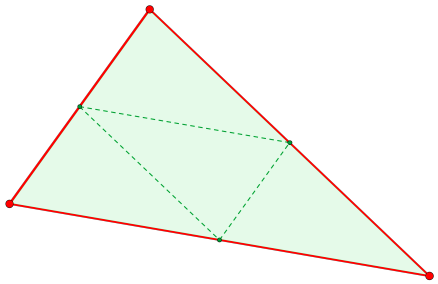

Figure 16: *process to subdivide a triangle of our mesh*

The curves converge quite rapidly after a given number of subdivision steps. We thus stop the subdivision process when the differences between the curves is small enough. However, small triangles require a small the time step to avoid oscillations (which slows down convergence). A good trade-off has then to be found between the number of subdivisions and the precision, in order to obtain enough accuracy but with sufficiently fast algorithms. Increasing the number of subdivision steps beyond this level does not improve precision, which led us to stop the subdivision process at 16.

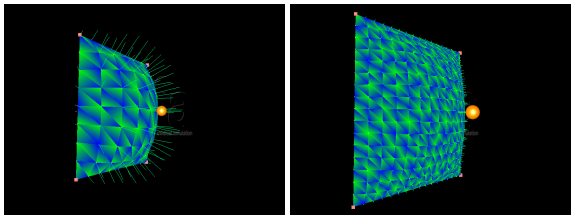

Figure 17: *Different levels of subdivision*

Using the SOFA framework, the whole force vs displacement curves of AFM on a single plane is computed in less than a minute with sufficient precision of 1E-3 .

5. Results and Discussion

5.1. Efficiency

We need fast algorithms because we are seeking at the same time precision and sufficiently smooth curves (typically a hundred of static equilibria computed to plot one curve).

We first used a structure with a mesh that is roughly uniform. In this case, the simulation converges quite rapidly: less than a minute to get each static equilibrium with high precision. However, the mesh deformation near the probe is unrealistic; in particular contact is lost between the probe and the structure because the triangles are too large.

Therefore we refined the mesh near the probe. The great difference in triangle size in the mesh makes it necessary to use an accurate linear solver with a very low error. Computing a single equilibrium configuration then takes several minutes.

5.2. Force-displacement curves

To study the sensitivity of the meristem model to mechanical factors, we plotted many force versus displacement curves, with (turgid state) or without internal pressure (plasmolyzed state), with different positions of the probe.

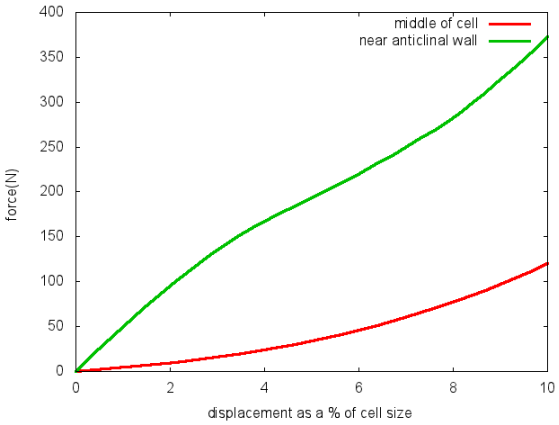

Figure 18: *Without pressure: indentation in the cell middle or at the edge*

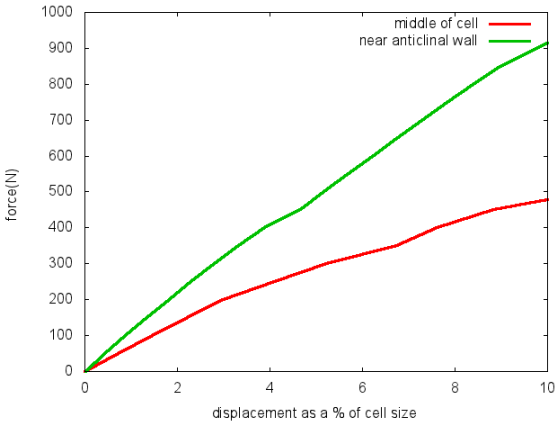

Figure 19: *With pressure: indentation in the cell middle or at the edge*

Inspection of these curves shows that the higher the Young modulus, or the pressure, the higher the force needed to indent down to the same depth. In the pressurized state, curves are roughly linear, with a higher slope near near cell edges

(near anticlinal wall, i.e. walls perpendicular to the surface). In the unpressurized state, the curves are nonlinear, also with a higher average slope near anticlinal walls. We also observe higher differences due to the structure at higher forces and higher displacement when no pressure is applied, while the pressurized state tends to make the curves more uniform regardless of the inner cell walls, which means that we are more sensitive to the pressure than to the elastic modulus in these states. Curves in pressurized state tend to be more linear too.

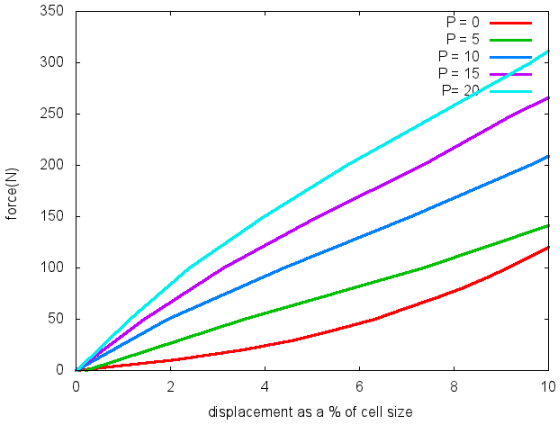

Figure 20: *Indentation in the cell middle, for different pressure values*

5.3. Range of parameters

As potentially thousands of degrees of freedom are involved in such 3D model, the problem of fitting physical parameters with respect to simulation and experimental data is often ill-conditioned and not invertible. However, dimensional analysis allows us to compare the ratio between forces and displacement, obtaining by solving many direct problems.

To get non-dimensional parameters we scaled the forces, F, with respect to Young Modulus and cell length, and the indentation, I, with the cell length :

$$[F] = \frac{F}{EL^2}$$

$$[I] = \frac{I}{L}$$

Experimental data without internal pressure (plasmolyzed state) were obtained by [PBG*11], where a typical displacement of $0.5\mu m$ was observed for a given force of around $1\mu N$. Replacing these parameters in $\frac{[F]}{[I]}$ gives us around the same value as our model, where, for a typical displacement of 10% of cell size also, we need an amount of force of around 400N, for a Young modulus of 1000Pa.

Our model is thus positioned in an acceptable range of values.

5.4. Concluding remarks

Exploring the space of parameters from the model indicates that different factors play a major role in AFM measurements. The key factors as shown by the force-displacement curves are :

- tip size of the AFM,
- properties of the structure, i.e. elastic modulus, turgor pressure,
- localization of indentation : near anticlinal walls or in the middle of cells.

However these factors are combined, which means that experiments require a careful interpretation, since none of these parameters can be isolated from the others to entirely explain the curves obtained. The framework that we present here allows a comprehensive exploration of all assumptions.

Acknowledgements

To the whole Sofa team for their everyday support, especially Benjamin Gilles for outstanding plugins. To P. Das, J. Chopard and F. Boudon for the realistic structure of meristem. To O. Ali for suggesting dimensional analysis.

References

[BCA*14] BOUDON F., CHOPARD J., ALI O., GILLES B., HAMANT O., BOUDAOUD A., TRAAS J., GODIN C.: A computational framework for 3d mechanical modeling of plant morphogenesis with cellular resolution (under review). 2014. 2

[BW98] BARAFF D., WITKIN A.: Large steps in cloth simulation. *Computer Graphics (Proc. SIGGRAPH)* (1998). 4

[CRLM*04] COEN E., ROLLAND-LAGAN A.-G., MATTHEWS M., BANGHAM J. A., PRUSINKIEWICZ P.: The genetics of geometry. *Proceedings National Academy of Sciencs USA 101* (2004), 4728–35. 1

[FCS*12] FERNANDES A. N., CHEN X., SCOTCHFORD C. A., WALKER J., WELLS D. M., ROBERTS C. J., EVERITT N. M.: Mechanical properties of epidermal cells of whole living roots of arabidopsis thaliana : An atomic force microscopy study. *Physical Review E* (2012). 2

[FDD*12] FAURE F., DURIEZ C., DELINGETTE H., ALLARD J., GILLES B., MARCHESSEAU S., TALBOT H., COURTECUISSE H., BOUSQUET G., PETERLIK I., COTIN S.: SOFA: A Multi-Model Framework for Interactive Physical Simulation. In *Soft Tissue Biomechanical Modeling for Computer Assisted Surgery*, Payan Y., (Ed.), vol. 11 of *Studies in Mechanobiology, Tissue Engineering and Biomaterials*. Springer, June 2012, pp. 283–321. URL: http://hal.inria.fr/hal-00681539, doi:10.1007/8415_2012_125. 2

[FDM*10] FERNANDEZ R., DAS P., MIRABET V., MOSCARDI E., TRAAS J., VERDEIL J.-L., MALANDAIN G., GODIN C.: Imaging plant growth in 4d: robust tissue reconstruction and lineaging at cell resolution. *Nature Methods 7* (2010), 547–53. 2, 3

[Gei06] GEITMANN A.: Experimental approaches used to quantify physical parameters at cellular and subcellular levels. *American Journal of Botany* (October 2006), 1380–1390. 2

[Joh87] JOHNSON K.: *Contact mechanics*. Cambridge University Press, 1987. 2

[KWK*12] KIERZKOWSKA A.-L. R., WEBER A., KOCHOVA P., FELEKIS D., B.J.NELSON, KUHLEMEIER C., SMITH R. S.: Cellular force microscopy for in vivo measurements of plant tissue mechanics. *Plant Physiology* (April 2012). 2

[LBT08] LEE D., BARBER J. R., THOULESS M. D.: Indentation of an elastic half space with material properties varying with depth. *International Journal of Engineering Science* (2008), 1274–1283. 2

[LL70] LANDAU L. D., LIFCHITZ E. M.: *Theory of Elasticity*. Pergamon Press, 1970. 6

[MBB13] MILANI P., BRAYBROOK S. A., BOUDAOUD A.: Shrinking the hammer : micromechanical approaches to morphogenesis. *Journal of Experimental Botany* (2013). 2

[MDBH11] MIRABET V., DAS P., BOUDAOUD A., HAMANT O.: The role of mechanical forces in plant morphogenesis. *Annual Reviews of Plant Biology 62* (2011), 365–85. 1

[MGT*11] MILANI P., GHOLAMIRAD M., TRAAS J., ARNEODO A., BOUDAOUD A., ARGOUL F., HAMANT O.: In vivo analysis of local wall stiffness at the shoot apical meristem in arabidopsis using atomic force microscopy. *The Plant Journal* (2011). 2

[MMC*14] MILANI P., MIRABET V., CELLIER C., ROZIER F., HAMANT O., DAS P., BOUDAOUD A.: Matching patterns of gene expression to mechanical stiffness at cell resolution through quantitative tandem epifluorescence and nano-indentation. *Plant Physiology* (2014), 114.237115. 2

[Nik92] NIKLAS K.: *Plant Biomechanics, An Engineering Approach to Plant Form and Function*. The University of Chicago Press, 1992. 1, 2

[PBG*11] PEAUCELLE A., BRAYBROOK S., GUILLOU L. L., BRON E., KUHLEMEIER C., HÃűFTE H.: Pectin-induces changes in cell wall mechanics underlie organ initiation in arabidopsis. *Current Biology* (October 2011), 1720–1726. 2, 9

[PMT06] P.VOLINO, MAGNENAT-THALMANN N.: Simple linear bending stiffness in particle systems. *Eurographics/ ACM SIGGRAPH Symposium on Computer Animation* (2006). 6

[RKS13] ROUTIER-KIERZKOWSKA A.-L., SMITH R. S.: Measuring the mechanics of morphogenesis. *Current Opinion in Plant Biology* (February 2013), 25–32. 2

[RRS*12] RADOTIC K., RODUIT C., SIMONOVIC J., HORNITSCHEK P., FRANKHAUSER C., MUTAVDZIC D., STEINBACH G., DIETLER G., KASAS S.: Atomic force microscopy stiffness tomography on living arabidopsis thaliana cells reveals the mechanical properties of surface and deep cell-wall layers during growth. *Biophysical Journal* (August 2012), 386–394. 2

[RSD*09] RODUIT C., SEKATSKI S., DIETLER G., CATSICAS S., LAFONT F., KASAS S.: Stiffness tomography by atomic force microscopy. *Biophysical Journal* (2009), 674–677. 2

[SSIF07] SIFAKIS E., SHINAR T., IRVING G., FEDKIW R.: *Hybrid Simulation of Deformable Solids*. ACM Transactions on Graphics (Proc. SIGGRAPH)/Eurographics Symposium on Computer Animation, 2007. 5

[VAVB12a] VELLA D., AJDARI A., VAZIRI A., BOUDAOUD A.: Indentation of ellipsoidal and cilindrical elastic shells. *Phisical Review Letters* (October 2012). 2, 6

[VAVB12b] VELLA D., AJDARI A., VAZIRI A., BOUDAOUD A.: The indentation of pressurized elastic shells : from polymeric capsules to yeast cells. *Journal of the Royal Society Interface* (March 2012), 448–455. 2

[ZC67] ZIENKIEWICZ O. C., CHEUNG Y. K.: *The finite element method in structural and continuum mechanics*. McGraw-Hill Publ, 1967. 4